Mathematical Biology

L.J. Cummings · S.L. Waters · J.A.D. Wattis · S.J. Graham

The effect of ureteric stents on urine flow: Reflux

Abstract. If the ureter becomes blocked, the resultant increased pressure may be relieved by inserting a *double-J stent* (a polymer tube, usually punctuated with holes). A major clinical problem associated with stent use is reflux (retrograde flow of urine from the bladder to the kidney), which may result in infections, scarring, and even renal failure.

We develop a mathematical model, treating the ureter as an elastic tube and the stent as a permeable rigid tube within it. We investigate how the number of holes in the stent wall affects the total amount of reflux that occurs when bladder pressure rises, by considering the limits of a highly-permeable stent, and an impermeable stent. We find that, in the scenarios we consider, the highly-permeable stent gives rise to less total reflux than the impermeable one.

1. Introduction

The urinary tract is a conduit, storage and modification system for urine excreted by the kidney. When produced, urine collects in the funnel-shaped renal pelvis of the kidney, and passes down the ureter to the bladder, where it is stored at low pressure until voiding is achieved. Urine is mainly water and contains salts, urea and a little protein. It is usually supersaturated, but in normal individuals inhibitors of crystallisation keep it in a liquid state [12]. The urine in the bladder is more concentrated and of higher pH than the urine in the renal pelvis and, while levels of bacteria in urine are normally very low (less than 10^3 per mm^3; 'sterile'), bladder levels are usually higher than in the renal pelvis since the bladder is nearer the external environment. The renal pelvis has a very low bacterial tolerance, and is thus very susceptible to infection.

In a healthy system, rhythmic coordinated contractions of the ureter (peristalsis) push urine down the ureter to the bladder at a normal flow rate of about 0.5 ml min^{-1} for each kidney/ureter (although in disease states such as diabetes insipidus the rate may be as high as 4 ml min^{-1}) [1,8,9]. The ureter may become blocked, however, either internally (*e.g.* by a kidney stone) or by external compression (*e.g.* from a tumour) and an obstruction can rapidly become life threatening, either due to increased intrarenal pressure (which may stop urine production and

L.J. Cummings, S.L. Waters, J.A.D. Wattis: School of Mathematical Sciences, University of Nottingham, Nottingham NG7 2RD, U.K.
e-mail: Linda.Cummings@nottingham.ac.uk

S.J. Graham: Barnet & Chase Farm Hospitals NHS Trust, The Ridgeway, Enfield, Middlesex, EN2 8JL, U.K.
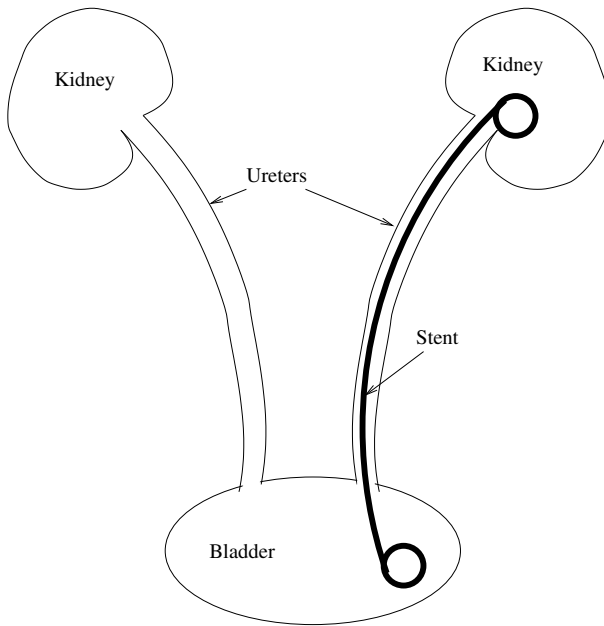
Fig. 1. Schematic showing the upper urinary tract with a stent in one ureter.

over time cause kidney failure) or by causing an infection. Ideally, the obstruction should be removed, but if this is not possible, the pressure must be relieved. This may be done by direct drainage of the kidney (a nephrostomy), or via the insertion of a stent.

A number of different stent designs are available clinically [14]: double-J stents made of polymers (considered here), which extend the entire length of the ureter; and a range of shorter metal stents, which sit at the blockage site. The double-J stent is a tube, usually punctuated with holes, with a typical internal diameter of 1mm and length of 25cm. It is relatively pliable longitudinally (floppy), but difficult to compress radially. Curls at each end keep the lower end in the bladder and the upper end in the renal pelvis [5].

Two major problems are commonly associated with stent use.

(i) Reflux. During normal function, when bladder pressure rises (*e.g.* when the bladder is full, or during urination) the bladder-ureter junction (the vesico-ure-teric junction or VUJ) contracts and closes. After stenting, however, the VUJ is not able to close fully because of the presence of the stent. Moreover, intro-duction of the stent causes the ureter quickly to lose muscle tone (this is linked to the suppression of peristalsis in a stented ureter; see below), and the VUJ in a stented ureter thus remains dilated [14]. This means that bladder urine is able to travel back up the ureter to the renal pelvis. This is known as *reflux* [2] and may result in renal infections such as pyelonephritis and subsequent

scarring, and, over time, a fall off in renal function.[1] Stented patients are particularly prone to high bladder pressures as the lower curl of the stent rests on a sensitive part of the bladder called the trigone. This causes irritation (as well as unpleasant symptoms including increased urinary frequency, pain and haematuria), leading to pressure rises in the bladder due to muscle contractions (referred to as *twitches*). Furthermore, and for reasons which do not appear to be fully understood, the presence of a stent abolishes peristalsis [2, 11, 13, 14]. For example, the study of [13], also cited in [14], found that peristalsis was rarely seen in stented patients before 2 months, after which it reappeared in one third of patients, but was weak in quality. Thus flow in the ureter is immediately susceptible to pressure fluctuations in the bladder, again resulting in an increased likelihood of reflux.

(ii) Encrustation. Around 15%–20% of patients require a stent to be inserted indefinitely, but over several months, the stent can become *encrusted* with crystalline deposits of salts from urine which, as well as causing discomfort, can lead to inflammation and further blockage. While a certain amount of encrustation can be tolerated on the bladder end of the stent, encrustation within the renal pelvis is extremely problematic, as stent removal becomes difficult and may even require an open operation [6, 14].

For those 80–85% of patients only requiring a stent in the short term, reflux (as defined above) is a far more serious issue than encrustation. However, the two issues are closely linked. The insertion of a stent leads to the potential for introducing bacteria into the system. As well as the obvious infection risk, certain bacteria, *e.g. Proteus* spp and *Morganella morganii* (commonly found in the urine) produce *urease*, an enzyme that catalyses the hydrolysis of urea in the urine to carbon dioxide and ammonia, thus elevating the urinary pH. The rate of encrustation (crystallisation) increases with pH; thus since both bacteria and pH levels are higher in the bladder, reflux can exacerbate encrustation within the renal pelvis.

Previous theoretical models of ureteric flow dynamics have focused on healthy ureteric function, in which the flow is driven by peristaltic contraction waves (see, for example, [1, 8, 9] and references therein). Since a double-J stent abolishes peristalsis, however, most of this work is not applicable here. In this paper we develop a simple mathematical model for the flow in a stented ureter. The ureter is modelled as an elastic tube, and the stent as a permeable rigid tube, both of the same length. The ureter is usually lobular or slit-like in cross-section (except when a fluid bolus passes through). When stented however, loss of muscle tone due to the suppression of peristalsis [2, 11, 14], and the higher-than-normal pressures resulting from the system still being partially blocked, combine to cause ballooning of the ureter wall [2]. It is therefore reasonable to restrict attention to the case of axisymmetric geometry. Moreover, without peristalsis, the ureter drains passively, the urine flow being driven only by the pressure difference between the renal pelvis and the bladder [14]. Usually (when the patient is standing or sitting) this pressure difference is purely

---

[1] We note that a 'non-reflux' stent design has been reported by Dauleh *et al.* [3], in which the lower end curl of the stent is replaced by a thread, so that the VUJ is no longer held open by the stent. However this design is not in widespread use.

hydrostatic due to the renal pelvis typically being 20cm above the bladder. However, twitches and voiding both increase bladder pressure considerably, increasing the likelihood of reflux.

The key dimensionless parameters in our model are the *stiffness* of the ureter wall (its resistance to stretching under pressure) and the *permeability* of the stent wall (a measure of how much fluid will flow out through the holes in the stent wall, relative to the amount that flows directly down the centre of the stent). We investigate flow in the stented ureter in different parameter regimes, and in particular, study situations in which reflux occurs.

2. Modelling

2.1. Physiological parameter values and definitions

Here we list the dimensional governing parameters of the system, with estimations of their physiological values. Stars denote dimensional quantities throughout.

μ^* = viscosity of urine, assumed to be that of water (0.654 g cm^{-1} s^{-1} at 40° C).
ρ^* = density of urine, again assumed to be that of water (1 g cm^{-3}).
P_b^* = pressure in the bladder. Usually this is 2–5 cm H$_2$O, but during a twitch or on voiding it can reach 30 cm H$_2$O or 50 cm H$_2$O respectively.
P_k^* = pressure in the renal pelvis $\approx$ 20 cm H$_2$O in stented patients ($\approx$ 4 cm H$_2$O unstented).
L^* = total length of ureter (and stent) $\approx$ 25cm.
a^* = internal radius of stent $\approx$ 1mm.
b^* = internal radius of ureter, usually less than 3mm.
b_a^* = ambient internal radius of ureter (when pressures inside and outside ureter are equal), here taken to be 2mm.
k^* = stiffness of ureter wall, in the sense defined in (2.3) $\approx$ 41-45cm H$_2$O mm^{-1} at typical voiding pressures (based on the data of [10]).
h^* = thickness of stent wall $\approx$ 0.5mm.
e^* = radius of holes in stent wall $\approx$ 0.25mm.
N = number of holes in stent wall $\approx$ 50.
n^* = number of holes per unit area in stent wall $\approx$ 3.18cm^{-2}.
λ^* = stent wall permeability, as defined by (2.2) (must be determined experimentally, or estimated as discussed later).

2.2. Preliminaries

Throughout this paper we assume that the stent-ureter system is axisymmetric. The basic geometry is sketched in figure 2. We use cylindrical polar coordinates (r^*, θ, z^*), with associated unit vectors (e_r, e_θ, e_z), where the z^*-axis lies along the centre of the stent (and ureter). The velocity of the fluid (urine, which being mainly water is assumed Newtonian) is represented by $u^* = u^*(r^*, z^*, t^*)e_z + v^*(r^*, z^*, t^*)e_r$. Gravity (represented by g^*) is assumed to act along the z^*-direction. (Even if it has a component perpendicular to this direction its effect will not
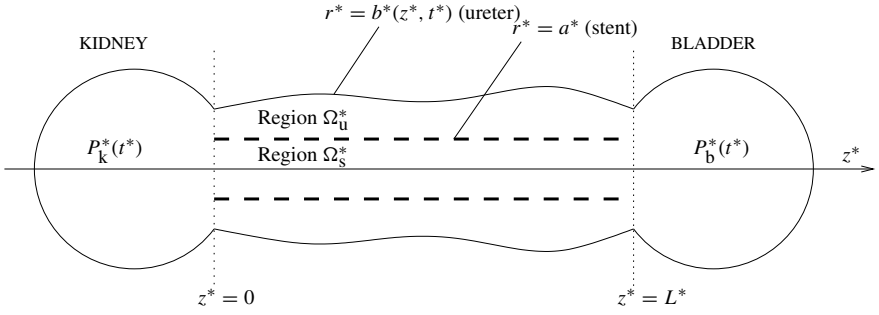
Fig. 2. Schematic showing axisymmetric coordinate system and definitions used.

enter the leading order equations in the r^*- and θ-equations, so it is simplest to assume this at the outset.) If the patient is lying down, the gravity parameter can be set to zero in the model. All our calculations for reflux during urination will be based on a standing/sitting patient (a 'best-case' scenario as far as reflux is concerned, since any refluxing urine has then to overcome the effect of gravity to reach the kidney).

The pressures in the stent interior (region Ω_s^*) and in the gap between the stent and the ureter wall (region Ω_u^*) are denoted by p_s^* and p_u^*, respectively (we will use 's' and 'u' elsewhere to distinguish between other quantities, such as velocity, in these two regions). The ambient pressure in the body outside the ureter p_{body}^* is taken to be hydrostatic, induced only by gravity. It proves convenient to work throughout with *reduced* pressures: $\widehat{p}^* = p^* - (\rho^* g^* z^* + p_c^*)$ for some constant p_c^*, as this removes gravity from the Navier-Stokes equations. The reduced pressure $\widehat{p}_{body}^*$ is then just a constant, which, by choosing

$$p_c^* = \left. p_{body}^* \right|_{z^*=0} \approx 4 \text{ cm } H_2O \tag{2.1}$$

(assuming the ambient body pressure at the renal pelvis is more or less the same as that in an unstented renal pelvis), is zero: $\widehat{p}_{body}^* \equiv 0$. Henceforth, when we say 'pressure', 'reduced pressure' is understood.

2.3. Flow through the permeable stent wall

Since the stent has holes in its side, urine will flow between the stent and the ureter if there is a pressure difference across the stent wall, as indicated in figure 3. The total flux through the stent wall will be linear in the pressure drop across the wall. Hence, assuming that the stent wall is thin, so that conditions on the outer and inner stent walls may both be applied at $r^* = a^*$, this gives conditions on the radial velocity v^* at the stent wall of the form:

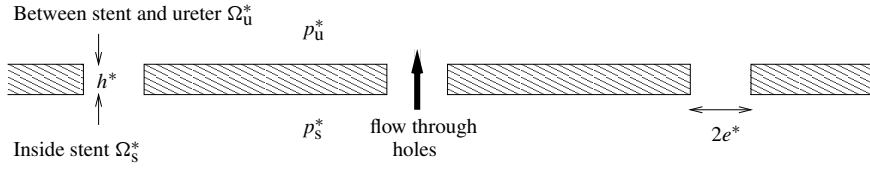$$v_u^* = \lambda^*(\widehat{p}_s^* - \widehat{p}_u^*) = v_s^* \quad \text{on } r^* = a^*, \tag{2.2}$$

Fig. 3. Flow through the permeable wall of the stent.

where λ^* is a measure of the wall permeability, which could be determined exper-imentally.[2] In any case, it seems reasonable to assume that λ^* will be a linear function of the number of holes per unit area in the stent wall, and it can clearly be regarded as an adjustable parameter in the model.

2.4. Compliant tube model of ureter

The flow in regions Ω_s^* and Ω_u^* is governed by the Navier-Stokes equations, subject to appropriate boundary conditions. At the ureter wall, $z^* = b^*(z^*, t^*)$, the no-slip condition states that the fluid velocity must equal the velocity of the ureter wall. We also assume the following simple law for the elastic ureter wall:

$$k^*(z^*)(b^*(z^*, t^*) - b_a^*(z^*)) = \widehat{p}_u^* \quad (\text{if } \widehat{p}_u^* > 0), \quad \text{on } r^* = b^*. \qquad (2.3)$$

Here, $b_a^*(z^*)$ denotes the 'ambient' state of the ureter wall, when the pressure within it tends to zero (which, recall, is the value of the pressure $\widehat{p}_{body}^*$ external to it); and the function $k^*(z^*)$ is a measure of how difficult it is to stretch the ureter radially, *i.e.* of the *stiffness* of the ureter. Allowing k^* to vary spatially allows us to model a blockage as a region where $k^*(z^*)$ is locally large (a large internal pressure is then required to increase the ureter radius in this region). We do not stipulate what happens if $\widehat{p}_u^* \leq 0$ as this never happens physiologically; but clearly $b^*(z^*, t^*)$ can never be less than a^* for a stented ureter (an unstented ureter can contract to closure during peristalsis).

Equation (2.3) is a linear approximation to a true nonlinear wall law, as illus-trated in figure 4. Obviously, different linearisations of the true law are appropriate in different situations. For low values of $(\widehat{p}_u^* - \widehat{p}_{body}^*)$ the slope of the appropriate tangent will be larger, leading to a lower value for the ureter stiffness k^*; and the converse applies for large pressures. If one knows the exact nonlinear law, then the choice of the point about which we linearise it (marked by A in figure 4) is dictated by a typical value of $\widehat{p}_u^*$ in the situation we wish to model. If there are large variations in $\widehat{p}_u^*$ then obviously the linear law will be less accurate, but in fact for most of our analysis the variations are only small, and the linear approximation we employ is quite accurate.

---

[2] We note that, if the flow through the holes is assumed to be Poiseuille – which will not be the case as the stent wall is not thick enough for such a flow to develop – an explicit expression $\lambda^* = \pi e^{*4} n^*/(8\mu^* h^*)$ may be obtained, where e^* and h^* are indicated in figure 3 and n^* is the number of holes per unit surface area. In the absence of experimental data, this may provide an order of magnitude estimate of the wall permeability.
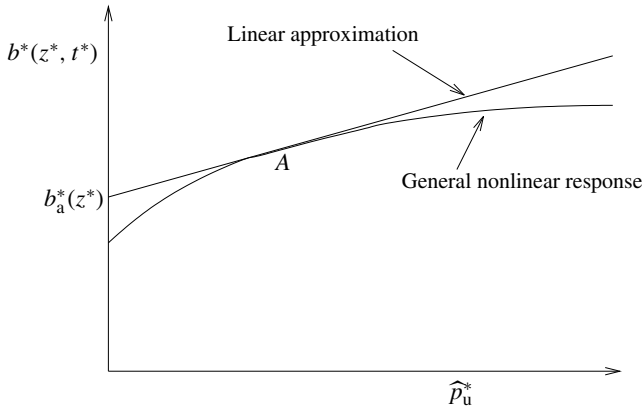
Fig. 4. Linear approximation to general wall law. The lower curve illustrates a general non-linear response of the ureter radius to the pressure drop across it; the upper line, with gradient $1/k^*(z^*)$, represents the linear wall response we adopt. The point of tangency, A, will be chosen such that the corresponding pressure drop is in the physiological regime we wish to model.

Since we are interested in the voiding situation, when most reflux occurs, we use a linearisation about a typical voiding pressure and ureter radius. If we assume (as stated earlier) that the ambient (absolute) pressure in the body at the renal pelvis is around the same as that in the unstented renal pelvis, *i.e.* 4 cm H_2O, then based on the data of §2.1, the reduced pressure in the renal pelvis is around 16 cm H_2O (and only a little higher in the bladder) when voiding, hence we take 16 cm H_2O as a typical pressure drop across the ureter wall in this situation.

We estimate the physiological value of k^* using the data of Knudsen *et al* [10] obtained from pig ureters. In this *in vivo* study, a balloon is used to inflate the pigs' ureters, and the inflation pressure p^* (in cm H_2O) and balloon cross-sectional area A^* (in mm^2) are measured simultaneously, and plotted. We estimate the slope of their graph at the relevant pressure to be $S^* = 2.96$ cm H_2O mm^{-2}. Then, since

$$S^* = \frac{\Delta p^*}{\Delta A^*} = \frac{\Delta p^*}{\pi (b^* + b_a^*)(b^* - b_a^*)},$$

we find that

$$(b^* - b_a^*) \left[\pi (b^* + b_a^*) S^* \right] = \Delta p^*.$$

Comparing with our wall law (2.3), we may identify k^* with the quantity in square brackets on the left-hand side. The data of [10] gives an ambient ureter radius b_a^* of around 2 mm, and a radius at $\Delta p^* = 16$ cm H_2O of $b^* \approx 2.4$ mm. Thus we arrive at the estimate

$$k^* = 41 \text{cm } H_2O \text{ mm}^{-2}. \tag{2.4}$$

At the permeable stent wall $r^* = a^*$ we assume no tangential slip of fluid on either side of the stent wall: $u_s^* = 0 = u_u^*$ (this is justified since the holes occupy a very small fraction of the stent wall surface area); and condition (2.2) also holds.

Finally, we must also impose boundary conditions at the ends of the stent, $z^* = 0$ (the kidney) and $z^* = L^*$ (the bladder). It seems clear that the pressure within the stent, $\widehat{p}_s^*$, must be equal to the kidney and bladder pressures, $\widehat{P}_k^*(t^*)$ and $\widehat{P}_b^*(t^*)$, at the respective ends. Since the pressure in the ureter, $\widehat{p}_u^*$, is related to the ureter radius through the boundary condition (2.3), we must choose whether to prescribe $\widehat{p}_u^*$, b^*, or some relation between them, at the ends. As mentioned in the Introduction, the ureteric wall quickly becomes passive after insertion of the stent (muscle tone is lost due to the lack of peristalsis), so the VUJ cannot contract around the stent but remains flaccid and dilated [14]. Hence we assume that the pressure $\widehat{p}_u^*$ in the region between ureter and stent is also equal to the kidney and bladder pressures at the respective ends, the ureter radius being free to adapt to these pressure conditions.

2.5. Nondimensionalisation

We nondimensionalise the Navier-Stokes equations, scaling z^* with L^*, and r^*, b^* and b_a^* with the stent radius $a^* = \epsilon L^*$ ($0 < \epsilon \ll 1$). Pressures are scaled with $\widehat{\Pi}^*$, a typical value of the pressure in the kidney (which, following the discussion above we will take to be 16 cm H_2O); the velocity component u^* with $U^* = \widehat{\Pi}^* a^{*2}/(\mu^* L^*)$ (to give a leading-order balance in the z-component of the Navier-Stokes equations), and v^* with $V^* = \epsilon U^*$ (to give a balance in the continuity equation). Time is scaled with L^*/U^*. If absolute pressures are also scaled with $\widehat{\Pi}^*$ then absolute and reduced pressures are related by $\widehat{p} = p - p_c - z\text{Bo}$, where $\text{Bo} = \rho^* g^* L^*/\widehat{\Pi}^*$ is the Bond number, and $p_c = p_c^*/\widehat{\Pi}^*$, with p_c^* as defined in (2.1).

Due to the tiny aspect ratio of the system $\epsilon \ll 1$, and the smallness of the reduced Reynolds number $\epsilon \text{Re} = \epsilon \rho^* U^* L^*/\mu^*$, lubrication theory is applicable. To leading order in ϵ the dimensionless Navier-Stokes equations are

$$\frac{\partial \widehat{p}_{s,u}}{\partial z} = \frac{1}{r}\frac{\partial}{\partial r}\left(r\frac{\partial u_{s,u}}{\partial r}\right), \tag{2.5}$$

$$\frac{1}{r}\frac{\partial}{\partial r}(rv_{s,u}) + \frac{\partial u_{s,u}}{\partial z} = 0, \tag{2.6}$$

where $\widehat{p}_{s,u}(z,t)$ is independent of r.

Under the assumptions of lubrication theory, the leading-order motion of the ureter wall is in the radial direction only, and the boundary conditions at the ureter wall become:

(a) $u_u = 0$,   (b) $v_u = \dfrac{\partial B}{\partial t}$,   (c) $\widehat{p}_u = K(B - B_a)$,   on $r = B(z,t)$, (2.7)

where $K(z) = \epsilon L^* k^*(L^* z)/\Pi^*$ and $B(z,t) = b^*(L^* z, L^* t/U^*)/(\epsilon L^*)$ are the dimensionless ureter stiffness and radius respectively ($B_a(z) = b_a^*(L^* z)/(\epsilon L^*)$).

In fact, since $\widehat{p}_u$ is independent of r, (2.7)(c) gives the pressure throughout Ω_u. Using the value of k^* given by (2.4), we estimate the value of the parameter K (for a healthy porcine ureter) as $K = 2.6$. At the stent wall we have

$$\text{(a) } u_u = 0 = u_s, \quad \text{(b) } v_u = \frac{\Lambda}{16}(\widehat{p}_s - \widehat{p}_u) = v_s, \quad \text{on } r = 1, \tag{2.8}$$

where $\Lambda = 16\lambda^*\mu^*/(L^*\epsilon^3)$ is the dimensionless stent permeability, which may be regarded as an adjustable parameter.

Finally, following the discussion of boundary conditions at the ends of the stent, at $z = 0$ we have dimensionless pressures $\widehat{p}_s = \widehat{p}_u = \widehat{P}_k(t) \equiv P_k(t) - p_c$, and at $z = 1$ $\widehat{p}_s = \widehat{p}_u = \widehat{P}_b(t) \equiv P_b(t) - p_c - \text{Bo}$.

3. Evolution equations for the ureter radius and pressures

We now use the model (2.5)–(2.8) to derive a fourth-order system of nonlinear PDEs relating the fluid pressures in the stent and ureter, and the ureter radius. We can solve for $u_{s,u}$ using (2.5), (2.7)(a) and (2.8)(a):

$$u_s = \frac{1}{4}\frac{\partial \widehat{p}_s}{\partial z}(r^2 - 1), \quad u_u = \frac{1}{4}\frac{\partial \widehat{p}_u}{\partial z}(r^2 - 1 + C_1 \log r^2),$$

$$\text{where} \quad C_1 = -\frac{B^2 - 1}{\log B^2}. \tag{3.9}$$

The radial velocities $v_{s,u}$ are then given by (2.6) as

$$v_s = \frac{1}{16}\frac{\partial^2 \widehat{p}_s}{\partial z^2}r(2 - r^2), \tag{3.10}$$

$$v_u = -\frac{1}{16}\frac{\partial^2 \widehat{p}_u}{\partial z^2}r\left(r^2 - 2 + 2C_1(\log r^2 - 1)\right)$$
$$-\frac{1}{8}\frac{\partial \widehat{p}_u}{\partial z}\frac{\partial C_1}{\partial z}r(\log r^2 - 1) - \frac{f(z,t)}{16r}, \tag{3.11}$$

where we used $v_s = 0$ on $r = 0$, and $f(z,t)$ in v_u is a function of integration. Using (2.8)(b) in (3.10), the pressures $\widehat{p}_u$ and $\widehat{p}_s$ are related via:

$$\widehat{p}_u = \widehat{p}_s - \frac{1}{\Lambda}\frac{\partial^2 \widehat{p}_s}{\partial z^2}. \tag{3.12}$$

Conditions (2.7)(b) and (2.8)(b) on v_u allow us to eliminate $f(z,t)$ from (3.11), giving a single equation linking $B(z,t)$, $\widehat{p}_s$ and $\widehat{p}_u$ (C_1 defined in (3.9) depends only on $B(z,t)$), which, using (3.12), may be written in the form

$$16B\frac{\partial B}{\partial t} + \frac{\partial^2 \widehat{p}_u}{\partial z^2}B^2(B^2 - 2) + \frac{\partial^2 \widehat{p}_u}{\partial z^2} - \frac{\partial^2 \widehat{p}_s}{\partial z^2}$$
$$-2\frac{\partial}{\partial z}\left(\frac{\partial \widehat{p}_u}{\partial z}\frac{(B^2 - 1)}{\log B^2}\right)(B^2 \log B^2 - B^2 + 1) = 0. \tag{3.13}$$

Equation (2.7)(c) gives $B(z, t)$ in terms of $\widehat{p}_u$ and hence, using (3.12), in terms of $\widehat{p}_s$:

$$B = B_a + \frac{\widehat{p}_u}{K} \equiv B_a + \frac{1}{K}\left(\widehat{p}_s - \frac{1}{\Lambda}\frac{\partial^2 \widehat{p}_s}{\partial z^2}\right). \tag{3.14}$$

Equations (3.12)–(3.14) are the governing evolution equations. They may be reduced to a single equation by substituting in (3.13) for $\widehat{p}_u$ and B in terms of $\widehat{p}_s$, using (3.12) and (3.14), giving a single 4th-order nonlinear partial differential equation for the pressure in the stent, $\widehat{p}_s$. As noted below equation (2.8) we have boundary values for $\widehat{p}_s$ and hence, using (3.12), for $\partial^2 \widehat{p}_s/\partial z^2$ at $z = 0$, 1:

$$\widehat{p}_s = P_k(t) - p_c \equiv \widehat{P}_k(t), \qquad \frac{\partial^2 \widehat{p}_s}{\partial z^2} = 0, \quad \text{at } z = 0,$$

$$\widehat{p}_s = P_b(t) - p_c - \text{Bo} \equiv \widehat{P}_b(t), \qquad \frac{\partial^2 \widehat{p}_s}{\partial z^2} = 0, \quad \text{at } z = 1. \tag{3.15}$$

An initial condition on the pressure completes the system.

The two key dimensionless parameters in the model are the ureter stiffness $K(z)$, and the stent permeability Λ. The asymptotic limit of small K is not physiologically relevant according to the porcine data of Knudsen *et al.* [10]. Also, this limit would, by (2.7)(c) and (3.12), necessitate either (a) very small pressures (which, recall, were made dimensionless on a typical system pressure and must therefore be order one); or (b) very large ureter wall displacements, which are not physiologically sensible. The large-K limit may be relevant in an externally-compressed ureter, as noted earlier, though we do not consider this limit here. We may, however, consider the obvious limits of large and small stent permeability. Clinically, the most important aspect of the fluid dynamics is the possibility of reflux; hence we will investigate situations that lead to reflux, and quantify how much reflux occurs in each of the asymptotic regimes investigated.

4. Solutions for large permeability ($\Lambda \to \infty$)

Given that the estimate for λ^* provided by footnote 2 leads to $\Lambda \approx 117$ for a typical stent, we first consider the behaviour of the system as $\Lambda \to \infty$. Writing $B = B_0 + O(1/\Lambda)$, and similarly for $\widehat{p}_u$ and $\widehat{p}_s$, equations (3.12) and (2.7)(c) give:

$$\widehat{p}_{s0} = \widehat{p}_{u0} = K(z)(B_0(z, t) - B_a(z)); \tag{4.16}$$

Equation (3.13) then gives a second-order nonlinear PDE for $B_0(z, t)$:

$$16B_0\frac{\partial B_0}{\partial t} + B_0^2(B_0^2 - 2)\frac{\partial^2}{\partial z^2}[K(B_0 - B_a)] - 2(B_0^2 \log B_0^2 - B_0^2 + 1)$$

$$\times \frac{\partial}{\partial z}\left(\frac{(B_0^2 - 1)}{\log B_0^2}\frac{\partial}{\partial z}[K(B_0 - B_a)]\right) = 0. \tag{4.17}$$

The boundary conditions on B_0 come from the pressure conditions (3.15) at $z = 0, 1$ via (4.16):

$$B_0(0, t) = B_a + \frac{\widehat{P}_k(t)}{K(0)}, \quad B_0(1, t) = B_a + \frac{\widehat{P}_b(t)}{K(1)}, \tag{4.18}$$

and we also require the initial ureter shape $B_0(z, 0)$ (if the initial pressure distribution is specified then $B_0(z, 0)$ is given by (4.16)).

When the pressures $\widehat{P}_k(t)$ and $\widehat{P}_b(t)$ at the ends of the ureter have the same value, which by our nondimensionalisation we may take to be 1 without loss of generality, equations (4.16) and (4.17) have the obvious steady solution

$$\widehat{p}_{u0} = 1 = \widehat{p}_{s0}, \quad B_0(z) = B_a(z) + \frac{1}{K(z)}, \tag{4.19}$$

for arbitrary ureter stiffness $K(z)$. This steady state solution may be used to describe voiding (which easily lasts long enough for a nearly steady state to be set up), since then the pressures at either end of the ureter are nearly equal (see the parameter values given in §2.1).

4.1. Perturbations to the steady state

The solution (4.19) describing voiding is only approximate, and for a more accurate description, we can consider perturbations to this steady state. Since the flow is driven by the pressures in the renal pelvis and bladder, we consider small perturbations, of size δ ($0 < (1/\Lambda) \ll \delta \ll 1$), to $\widehat{P}_k$ and $\widehat{P}_b$. Writing

$$\widehat{P}_k(t) = 1 + \delta \widehat{P}_{k1}(t) + O(\delta^2), \quad \widehat{P}_b(t) = 1 + \delta \widehat{P}_{b1}(t) + O(\delta^2),$$
$$B(z, t) = (B_a(z) + 1/K(z)) + \delta B_1(z, t) + O(1/\Lambda, \delta^2), \tag{4.20}$$

($\widehat{P}_{k1}(t)$ and $\widehat{P}_{b1}(t)$ are specified), and similarly for $\widehat{p}_s$ and $\widehat{p}_u$, we substitute these expansions into (3.13) and (3.14) above, and obtain, at order δ:

$$16 B_0 \frac{\partial B_1}{\partial t} = \left(B_0^4 - \frac{2(B_0^2 - 1)^2}{\log B_0^2} \right) \frac{\partial^2}{\partial z^2} (K B_1)$$

$$+ 2(B_0^2 \log B_0^2 - B_0^2 + 1) \frac{\partial}{\partial z} \left(\frac{B_0^2 - 1}{\log B_0^2} \right) \frac{\partial}{\partial z} (K B_1) = 0, \quad (4.21)$$

where $B_0(z) = B_a(z) + 1/K(z)$. This is much simpler if both $B_a(z)$ and $K(z)$ are constant (K constant is a good approximation for an unobstructed ureter), since then we obtain the diffusion equation

$$\frac{\partial B_1}{\partial t} = D_\infty \frac{\partial^2 B_1}{\partial z^2}, \quad D_\infty = \frac{K}{16 B_0} \left[B_0^4 - \frac{2(B_0^2 - 1)^2}{\log B_0^2} \right], \tag{4.22}$$

which must be solved subject to boundary conditions

$$B_1(0, t) = \frac{\widehat{P}_{k1}(t)}{K}, \quad B_1(1, t) = \frac{\widehat{P}_{b1}(t)}{K}, \tag{4.23}$$

and an appropriate initial condition.

The diffusion coefficient D_∞, which depends only on K and B_a, is always positive for $K > 0$, $B_a \geq 1$, but has the asymptotic behaviour

$$D_\infty = \frac{K}{16 B_a}\left(B_a^4 - \frac{2(B_a^2 - 1)^2}{\log B_a^2}\right) + O(1) \quad \text{as } K \to \infty;$$

and $D_\infty = 1/(16 K^2) + O(1/(K^2 \ln K))$ as $K \to 0^+$. Solutions to this model are considered in §6.

5. Solutions for small permeability ($\Lambda \to 0$)

There are sometimes problems with stents fracturing *in vivo*, and it is conjectured by some urologists that the holes in the stent wall may be partly responsible for this [4,7]. This could be an argument in favour of an impermeable, or less permeable, stent, with no, or fewer, holes in the wall. However, reducing the permeability of the stent obviously affects the fluid dynamics in the ureter; in particular, the degree of reflux that occurs. Hence we study the limit $\Lambda \to 0$ in equations (3.12)–(3.14), with the aim of quantifying the differences in the flow dynamics, which may enable us to draw some conclusions as to the usefulness of the holes.

We make asymptotic expansions for the functions $\widehat{p}_s$, $\widehat{p}_u$ and B in powers of the small parameter Λ. Equation (2.7)(c) for the pressure in the ureter is unchanged; and for the pressure in the stent, at leading order (3.12) gives $\widehat{p}_{s0}$ varying linearly between the prescribed values at the ends:

$$\widehat{p}_{s0} = \widehat{P}_k(t) + z(\widehat{P}_b(t) - \widehat{P}_k(t)), \tag{5.24}$$

so that the leading-order flow in the stent is Poiseuille. As before we can derive a second-order nonlinear PDE for the leading order ureter radius, which is very similar to equation (4.17) for the large permeability case:

$$16 B_0 \frac{\partial B_0}{\partial t} + (B_0^2 - 1)^2 \frac{\partial^2}{\partial z^2}\left(K(B_0 - B_a)\right) - 2(B_0^2 \log B_0^2 - B_0^2 + 1)$$

$$\times \frac{\partial}{\partial z}\left(\frac{B_0^2 - 1}{\log B_0^2}\frac{\partial}{\partial z}\left(K(B_0 - B_a)\right)\right) = 0. \tag{5.25}$$

The boundary conditions at $z = 0$, 1 are exactly as in (4.18).

As in §4, when both end pressures $\widehat{P}_k(t)$ and $\widehat{P}_b(t)$ are equal to 1, (4.19) gives a steady solution to (5.25), about which we may perturb.

5.1. Perturbations to the steady state

We assume asymptotic expansions exactly as in (4.20), except that now the condition we impose on the relative sizes of the small parameters is $0 < \Lambda \ll \delta \ll 1$ (so that we can proceed beyond leading order in δ using just leading order in Λ). To order δ the pressures are then given by

$$\widehat{p}_{s0} = 1 + \delta\left(\widehat{P}_{k1}(t) + z(\widehat{P}_{b1}(t) - \widehat{P}_{k1}(t))\right) + O(\delta^2),$$
$$\widehat{p}_{u0} = 1 + \delta K(z) B_1 + O(\delta^2). \tag{5.26}$$

At order δ we obtain

$$16B_0\frac{\partial B_1}{\partial t} = \left(B_0^4 - 1 - \frac{2(B_0^2 - 1)^2}{\log B_0^2}\right)\frac{\partial^2}{\partial z^2}(KB_1)$$

$$+2(B_0^2 \log B_0^2 - B_0^2 + 1)\frac{\partial}{\partial z}\left(\frac{B_0^2 - 1}{\log B_0^2}\right)\frac{\partial}{\partial z}(KB_1), \quad (5.27)$$

which, if K is constant, simplifies to a diffusion equation analogous to (4.22):

$$\frac{\partial B_1}{\partial t} = D_0\frac{\partial^2 B_1}{\partial z^2}, \quad D_0 = D_\infty - \frac{K^2}{16(K+1)}, \quad (5.28)$$

(D_∞ is defined in (4.22)), again subject to boundary conditions (4.23) and an appropriate initial condition.

6. Explicit solutions corresponding to voiding

We now consider some explicit solutions to equations (4.22) and (5.28). Recall that these two models describe the ureter shape during voiding (in the large- and small-permeability limits respectively), when the pressures in bladder and renal pelvis are nearly equal, differing only by an amount of $O(\delta)$ ($0 < \delta \ll 1$). Finding physiologically-relevant solutions to these models enables us to calculate explicitly the amount of reflux that occurs in the two limiting cases, and make a comparison between them.

6.1. Similarity solutions

As is well-known, equations (4.22) and (5.28) have similarity solutions of the form:

$$B_1(z, t) = c_1\mathrm{erf}(\eta) + c_2; \quad \eta = \frac{(z + z_0)}{2\sqrt{D(t + t_0)}}, \quad \mathrm{erf}(x) := \frac{2}{\sqrt{\pi}}\int_0^x e^{-s^2}ds,$$
$$(6.29)$$

where D denotes either D_∞ or D_0, for constants c_1, c_2, z_0 and t_0. Since t_0 represents only a choice of time origin, we set it to be zero. At the ends of the ureter B_1 is related to the pressure perturbations by (4.18):

$$B_1(0, t) = c_1\mathrm{erf}\left(\frac{z_0}{2\sqrt{Dt}}\right) + c_2 = \frac{\widehat{P}_{k1}(t)}{K}, \quad (6.30)$$

$$B_1(1, t) = c_1\mathrm{erf}\left(\frac{(1 + z_0)}{2\sqrt{Dt}}\right) + c_2 = \frac{\widehat{P}_{b1}(t)}{K}, \quad (6.31)$$

from which we see that such similarity solutions are possible only for pressure perturbations that vary in time in this specific manner.

Such a solution can be used to describe a small extra contraction of the bladder during voiding, where the bladder pressure suddenly rises to $1+\delta$, and is then maintained at this constant value: $\widehat{P}_{b1}(t) = 1$ for $t > 0$. If we impose $\widehat{P}_{k1}(0) = 0$ (no

initial perturbation to the pressure in the renal pelvis), then the similarity solution describing the behaviour of the ureter radius is

$$B(z, t) = B_a + \frac{1}{K} + \frac{\delta}{K}\left(1 - \mathrm{erf}\left(\frac{1-z}{2\sqrt{Dt}}\right)\right) + \begin{cases} O(\delta^2, 1/\Lambda) \\ O(\delta^2, \Lambda). \end{cases} \quad (6.32)$$

Although we have insisted that the excess bladder pressure remain constant, the restricted form of the solution means that we cannot also specify the excess pressure in the renal pelvis; it must increase in time according to:

$$\widehat{P}_k(t) = 1 + \delta\left(1 - \mathrm{erf}\left(\frac{1}{2\sqrt{Dt}}\right)\right) + \begin{cases} O(\delta^2, 1/\Lambda) \\ O(\delta^2, \Lambda). \end{cases} \quad (6.33)$$

Although we might expect the pressure within the renal pelvis to increase if reflux persists over long times, its behaviour in time will in reality be determined by a specific pressure-volume law within the renal pelvis, as the amount of fluid within it increases. However, we expect the above similarity solution to capture the general features.

The ureter radius is plotted as a function of (dimensionless) distance z along its length, for various times t and for various values of the permeability parameter K in figures 5(a)–10(a). The general features of the solution are always the same, though clearly as the ureter stiffness decreases, the variations in the ureter radius increase.
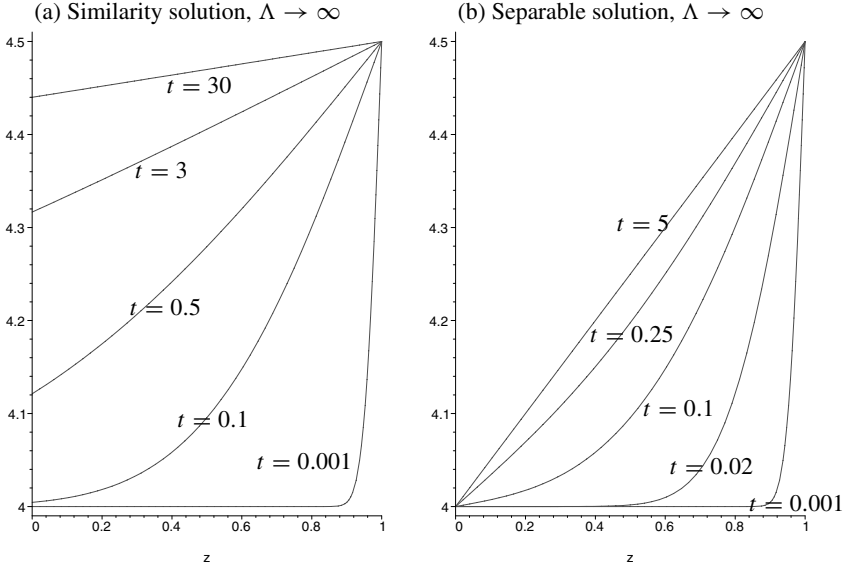

Fig. 5. The dimensionless ureter radius $B(z, t)$, plotted as a function of z at various times, for the similarity solution (6.32) and the separable solution (6.38) of equation (4.22) in the limit $\Lambda \to \infty$ (neglecting terms of order δ^2, $1/\Lambda$). Note the scaling of the axes. Parameter values $\delta = 0.25$, $B_a = 2$, $K = 0.5$ are taken, and 100 modes are used to plot the separable solution.
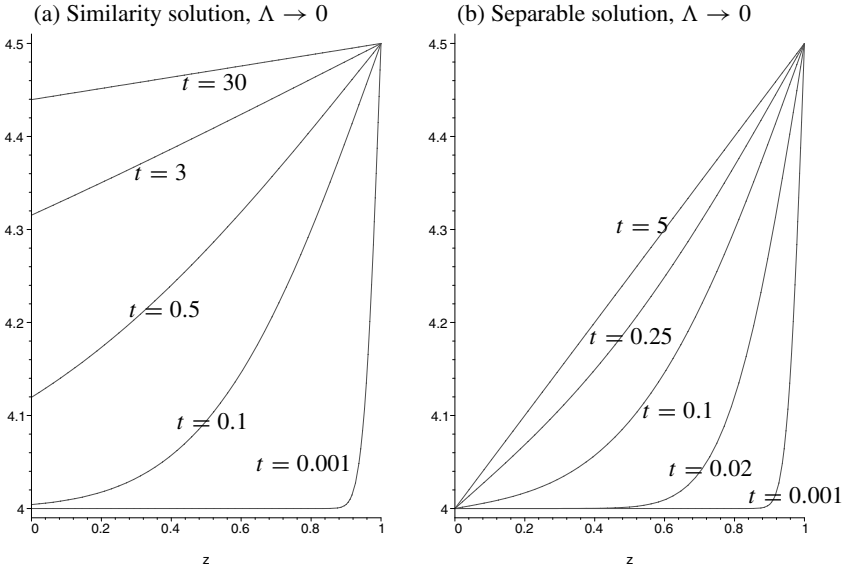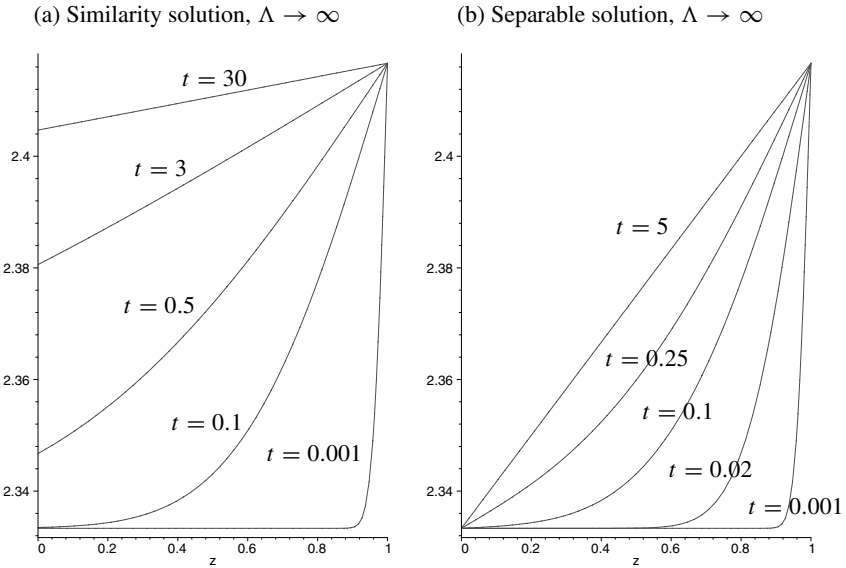
Fig. 6. The dimensionless ureter radius $B(z, t)$, plotted as a function of z at various times, for the similarity solution (6.32) and the separable solution (6.38) of equation (5.28) in the limit $\Lambda \to 0$ (neglecting terms of order δ^2, Λ). Note the scaling of the axes. Parameter values $\delta = 0.25$, $B_a = 2$, $K = 0.5$ are taken, and 100 modes are used to plot the separable solution.
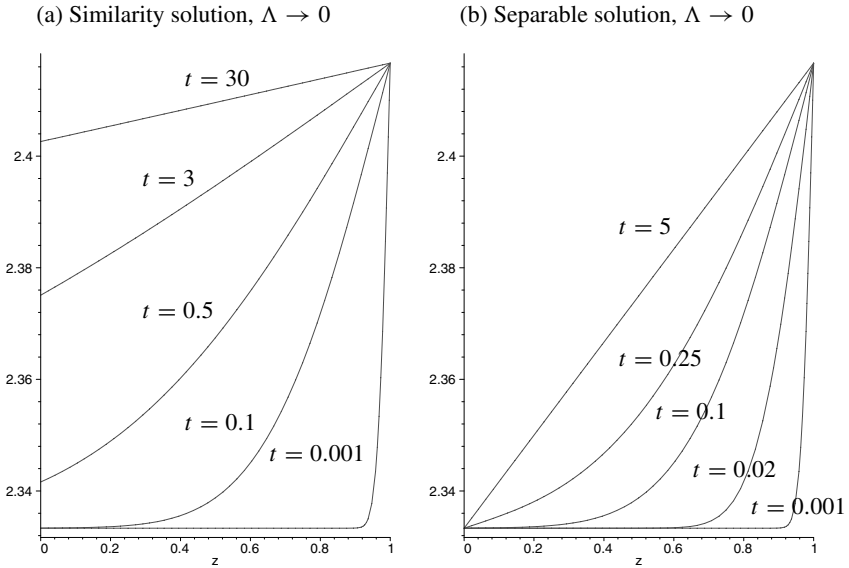

Fig. 7. As for figure 5 but with $K = 3$.

(a) Similarity solution, $\Lambda \to 0$

(b) Separable solution, $\Lambda \to 0$

$t = 30$

$t = 3$

$t = 0.5$

$t = 0.1$

$t = 0.001$

$t = 5$

$t = 0.25$

$t = 0.1$

$t = 0.02$

$t = 0.001$

Fig. 8. As for figure 6 but with $K = 3$.

(a) Similarity solution, $\Lambda \to \infty$

(b) Separable solution, $\Lambda \to \infty$

$t = 30$

$t = 3$

$t = 0.5$

$t = 0.1$

$t = 0.001$

$t = 5$

$t = 0.25$

$t = 0.1$

$t = 0.02$

$t = 0.001$
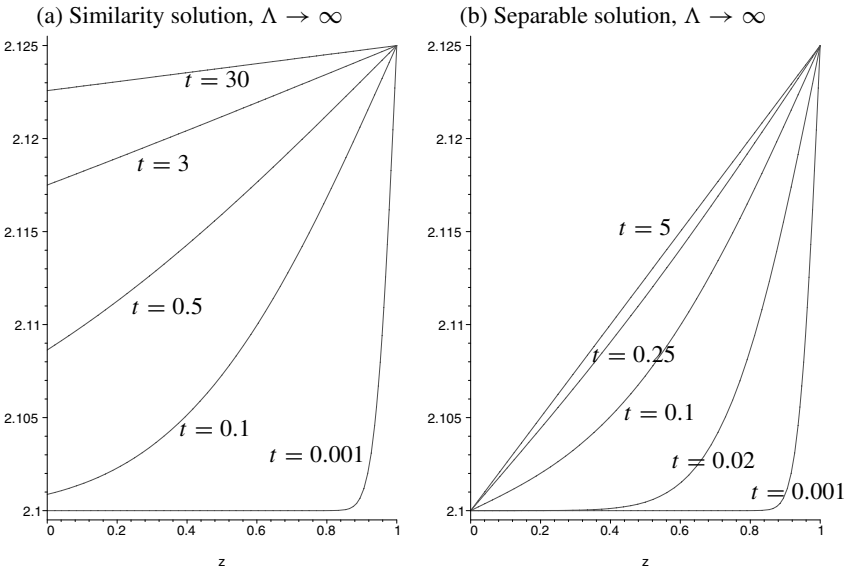
Fig. 9. As for figure 5, but with $K = 10$.

(a) Similarity solution, $\Lambda \to 0$
(b) Separable solution, $\Lambda \to 0$
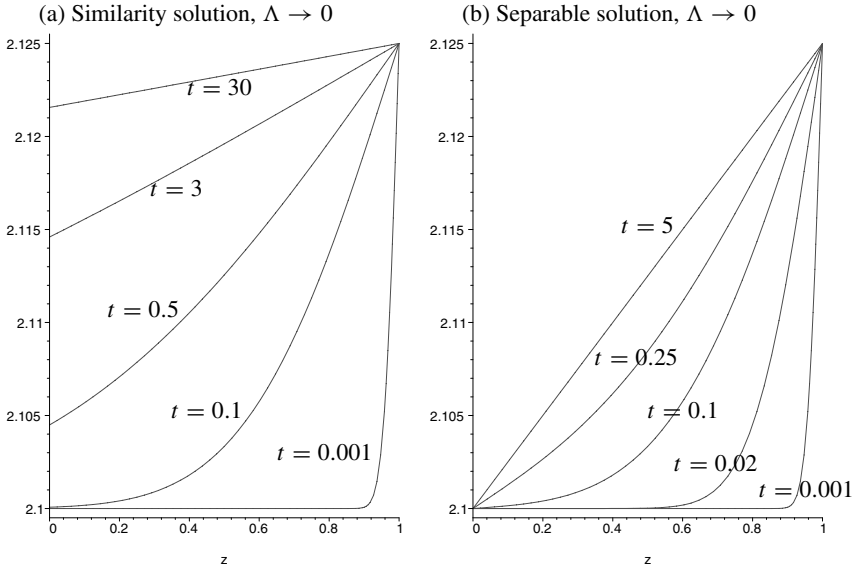
Fig. 10. As for figure 6, but with $K = 10$.

6.2. More general solutions

Although similarity solutions have the general properties we require, and have simple closed-form expressions, they restrict us to boundary conditions of a specific form at the bladder and kidney. If we wish to solve for more general end conditions, the solution will have a more complicated form.

In general, the bladder pressure during voiding will be a specified function of time (the patient controls this by how hard he squeezes the bladder). We assume for simplicity, as in the similarity solutions, that it is maintained constant, at a slightly higher level than the usual pressure in the renal pelvis. The pressure in the renal pelvis is constant before voiding, but as reflux occurs, will slowly rise. Hence we consider the boundary conditions:

$$\widehat{P}_{\mathrm{b}}(t) = 1 + \delta + O(\delta^2, 1/\Lambda), \quad \widehat{P}_{\mathrm{k}}(t) = 1 + \delta K g(t) + O(\delta^2, 1/\Lambda), \quad (6.34)$$

for some function g satisfying $g(0) = 0$ (no excess pressure in renal pelvis initially). The perturbation to the ureter radius is then given by the diffusion equation (4.22), together with the boundary conditions

$$B_1(0, t) = g(t), \quad B_1(1, t) = \frac{1}{K}, \quad (6.35)$$

and the initial condition

$$B(z, 0) = 0 \quad 0 \le z < 1. \quad (6.36)$$

The solution can be found by taking a Laplace transform in time:

$$B(z, t) = B_{\rm a} + \frac{1}{K} + \delta \left\{ \frac{z}{K} + \frac{2}{\pi K} \sum_{n=1}^{\infty} \frac{(-1)^n}{n} \exp(-Dn^2\pi^2 t) \sin(n\pi z) \right.$$

$$\left. + 2\pi D \sum_{n=1}^{\infty} (-1)^n n \sin n\pi (1-z) \int_0^t \exp(-Dn^2\pi^2\tau) g(t-\tau) d\tau \right\}$$

$$+ O(\delta^2, 1/\Lambda). \tag{6.37}$$

The above provides a solution for any choice of function $g(t)$ describing the variation of the excess pressure within the renal pelvis. If, as mentioned above, we wish to determine this pressure variation systematically (rather than make an *ad hoc* choice), we have first to work out the volume of reflux into the renal pelvis generated by this solution (for arbitrary g), and hence work out the resulting pressure within the renal pelvis at any given time, using a suitable pressure-volume law. This must be equal to $\widehat{P}_{\rm k}(t)$, given by (6.34), which will finally provide us with an equation to determine $g(t)$.

Since the principal goal of this paper is to determine qualitatively how the porosity of the stent affects the degree of reflux, we do not carry out this messy calculation here. Instead, we shall calculate the refluxes generated by two simple solutions: the similarity solution given in (6.32), and the solution (6.37) in the simplest case $g(t) = 0$:

$$B(z, t) = B_{\rm a} + \frac{1}{K} + \delta \left\{ \frac{z}{K} + \frac{2}{\pi K} \sum_{n=1}^{\infty} \frac{(-1)^n}{n} \exp(-Dn^2\pi^2 t) \sin(n\pi z) \right\}$$

$$+ O(\delta^2, 1/\Lambda) \tag{6.38}$$

(this solution can be obtained more easily by seeking separable modes). This solution is illustrated in figures 5(b)–10(b) for various values of K, in both limits $\Lambda \to \infty$ and $\Lambda \to 0$. As with the separable solution, the general features of the solution are the same in all cases, increases in K simply acting to supress the variations in the ureter radius. Physiologically, taking $g(t) = 0$ assumes that the renal pelvis provides a rather large reservoir for urine to reflux into, so that the pressure does not rise over time to the order considered. The volume of the renal pelvis is of the order of 10 cm^3, and numerical values for the total volume of reflux during voiding are given in §7.

7. Reflux

We now focus our attention on reflux, and its dependence upon the system parameters. The flux of urine $Q(z, t)$ through the ureter at any point z is defined by:

$$Q(z, t) = Q_{\rm s}(z, t) + Q_{\rm u}(z, t) \equiv \int_0^{2\pi} \int_0^1 u_{\rm s} r \, dr d\theta + \int_0^{2\pi} \int_1^{B_0} u_{\rm u} r \, dr d\theta. \tag{7.39}$$

The axial velocities within the stent-ureter system for the perturbed steady solutions of §4.1 ($\Lambda \to \infty$) and §5.1 ($\Lambda \to 0$) are found, using equations (3.9) and the results of §§4.1, 5.1, to be

$$\left. \begin{aligned} u_{\mathrm{s}}(r, z, t) &= \frac{\delta}{4} K \frac{\partial B_1}{\partial z}(r^2 - 1) + O(1/\Lambda, \delta^2) \quad \Lambda \to \infty \\ u_{\mathrm{s}}(r, z, t) &= \frac{\delta}{4}(\widehat{P}_{\mathrm{b1}} - \widehat{P}_{\mathrm{k1}})(r^2 - 1) + O(\Lambda, \delta^2) \ \Lambda \to 0 \end{aligned} \right\} 0 < r < 1, (7.40)$$

$$u_{\mathrm{u}}(r, z, t) = \frac{\delta}{4} K \frac{\partial B_1}{\partial z}\left(r^2 - 1 - \frac{B_0^2 - 1}{\log B_0^2} \log r^2\right)$$

$$+ \left.\begin{cases} O(1/\Lambda, \delta^2) \ \Lambda \to \infty \\ O(\Lambda, \delta^2) \quad \Lambda \to 0 \end{cases}\right\} 1 < r < B_0, \qquad (7.41)$$

where δ is the size of the perturbation to the bladder pressure, and all other quantities are as defined in the relevant sections. In particular, $B_0 = 1 + 1/K$. Thus

$$\begin{aligned} Q_{\mathrm{s}}(z, t) &= -\frac{\pi \delta K}{8} \frac{\partial B_1}{\partial z} + O(1/\Lambda, \delta^2) \quad \Lambda \to \infty, \\ Q_{\mathrm{s}}(z, t) &= -\frac{\delta \pi}{8}(\widehat{P}_{\mathrm{b1}} - \widehat{P}_{\mathrm{k1}}) + O(\Lambda, \delta^2) \ \Lambda \to 0, \end{aligned} \qquad (7.42)$$

$$Q_{\mathrm{u}}(z, t) = -\frac{2\delta \pi (1 + K) D_0}{K} \frac{\partial B_1}{\partial z} + \begin{cases} O(1/\Lambda, \delta^2) \ \Lambda \to \infty, \\ O(\Lambda, \delta^2) \quad \Lambda \to 0, \end{cases} \qquad (7.43)$$

with D_0 as defined in (5.28).

7.1. Comparison of reflux for permeable and non-permeable stents

Reflux for similarity solution (6.32) We evaluate the reflux at $z = 0$, that is, into the renal pelvis, since this is where it is most problematic. The ureter radius is given by (6.32), hence

$$\frac{\partial B_1}{\partial z} = \frac{1}{K\sqrt{\pi Dt}} \exp\left(-\frac{(1 - z)^2}{4Dt}\right) \quad \Lambda \to \infty, 0. \qquad (7.44)$$

Thus for $t > 0$ (7.42) and (7.43) give the total refluxes as

$$\left(\frac{-Q}{\delta}\right)_{\Lambda \to \infty} = \frac{2(K + 1)}{K^2}\sqrt{\frac{\pi D_\infty}{t}} \exp\left(-\frac{1}{4D_\infty t}\right), \qquad (7.45)$$

$$\left(\frac{-Q}{\delta}\right)_{\Lambda \to 0} = \frac{2(K + 1)}{K^2}\sqrt{\frac{\pi D_0}{t}} \exp\left(-\frac{1}{4D_0 t}\right) + \frac{\pi}{8}\mathrm{erf}\left(\frac{1}{2\sqrt{D_0 t}}\right). \quad (7.46)$$

For small times $t \ll 1$, the reflux is greater for the $\Lambda \to 0$ stent:

$$\left(\frac{-Q}{\delta}\right)_{\Lambda \to 0} - \left(\frac{-Q}{\delta}\right)_{\Lambda \to \infty} = \frac{\pi}{8} + O\left(\frac{1}{\sqrt{t}}\exp\left(-\frac{1}{4Dt}\right)\right) > 0,$$

and at large times also:

$$\left(\frac{-Q}{\delta}\right)_{\Lambda\to 0} - \left(\frac{-Q}{\delta}\right)_{\Lambda\to\infty} = \frac{2(1+K)}{K^2}\sqrt{\frac{D_\infty\pi}{D_0 t}}(\sqrt{D_\infty}-\sqrt{D_0}) + O\left(\frac{1}{t^{3/2}}\right).$$

The reflux-time curves for the specific cases $K = 0.5, 3, 10$ are shown in figures 11, 12 and 13, which demonstrate that there is less total reflux in the limit $\Lambda \to \infty$ (although for smaller values of K the difference in refluxes is only small).

The total reflux over time may be found by integrating the expressions (7.45) and (7.46) with respect to t. Clearly the integrals do not converge over infinite time, but for $T \gg 1$ we obtain:

$$\int_0^T \left(\frac{-Q}{\delta}\right)_{\Lambda\to\infty} dt = \frac{4(K+1)}{K^2}\sqrt{\pi D_\infty T} + O(1), \tag{7.47}$$

for the very permeable stent. For the non-permeable stent, for $T \gg 1$ we find

$$\int_0^T \left(\frac{-Q}{\delta}\right)_{\Lambda\to 0} dt = \frac{4(K+1)}{K^2}\sqrt{\pi D_\infty T}\sqrt{\frac{D_\infty}{D_0}} + O(1). \tag{7.48}$$

Comparing (7.47) and (7.48), since $D_\infty > D_0$, the total amount of fluid that has refluxed by time $t = T \gg 1$ is clearly larger for the non-permeable stent than for the permeable stent.
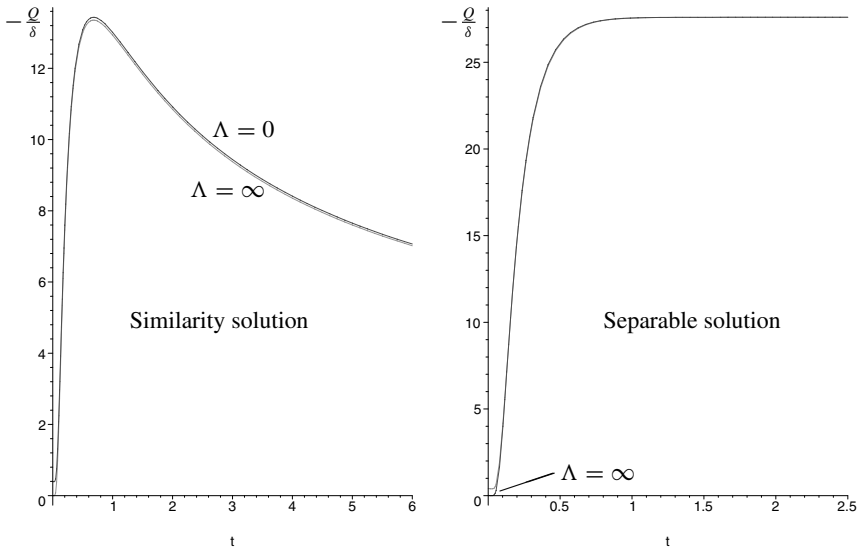

Fig. 11. Comparison of reflux over time for similarity and separable solutions when $\delta = 0.25$, $B_a = 2$ and $K = 0.5$. 100 modes are used when plotting the reflux for the separable solution. In both cases it is clear that the difference in reflux is small for this value of K.
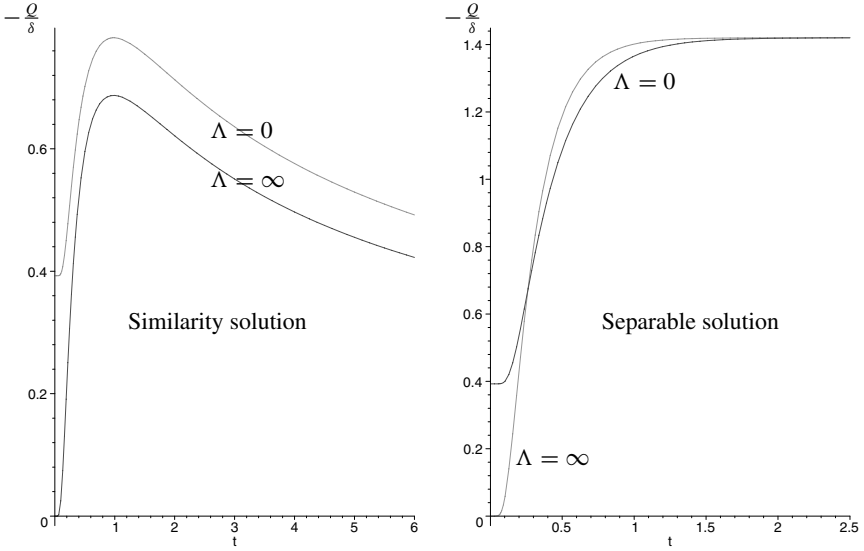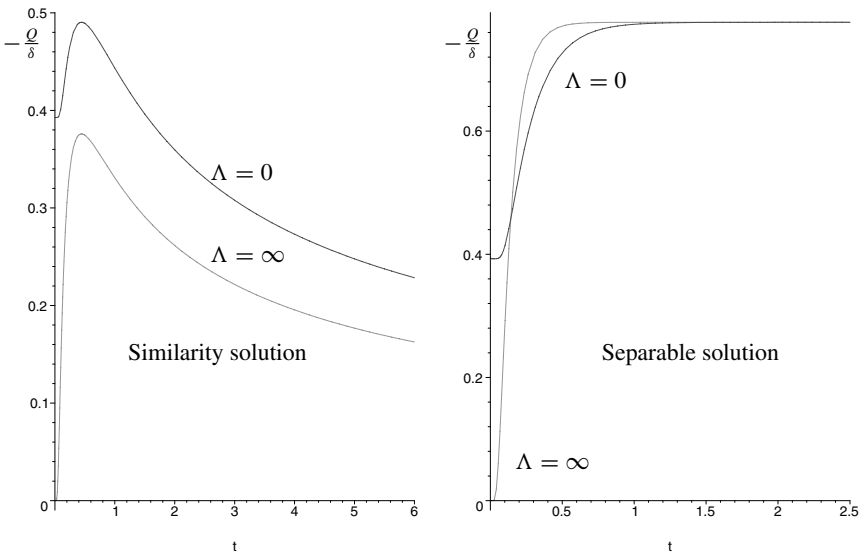
Fig. 12. Comparison of reflux over time for similarity and separable solutions when $\delta = 0.25$, $B_a = 2$ and $K = 3$. 100 modes are used when plotting the reflux for the separable solution.

Fig. 13. Comparison of reflux over time for similarity and separable solutions when $\delta = 0.25$, $B_a = 2$ and $K = 10$. 100 modes are used when plotting the reflux for the separable solution.

Dimensional total reflux The dimensional total reflux over a time T^* is given by

$$R^*(T^*) = \delta a^{*2} L^* \int_0^T \left(\frac{-Q}{\delta}\right) dt \approx 0.0625 \int_0^T \left(\frac{-Q}{\delta}\right) dt \text{ cm}^3, \quad (7.49)$$

using the values provided in §2.1, and $\delta = 0.25$. Considering different voiding scenarios with voiding times of $T^* = 5, 10, 20, 40\text{s}$, we arrive at dimensionless voiding times $T \approx 2.5, 5, 10, 20$. Performing the integral numerically for various K-values, we obtain the following values.

Over 5 seconds:

$$\begin{aligned}
K &= 0.5 \quad \Lambda \to \infty \quad R^*(5) = 1.72\text{cm}^3 \\
K &= 0.5 \quad \Lambda \to 0 \quad R^*(5) = 1.74\text{cm}^3 \\
K &= 3.0 \quad \Lambda \to \infty \quad R^*(5) = 0.090\text{cm}^3 \\
K &= 3.0 \quad \Lambda \to 0 \quad R^*(5) = 0.109\text{cm}^3 \\
K &= 10.0 \quad \Lambda \to \infty \quad R^*(5) = 0.046\text{cm}^3 \\
K &= 10.0 \quad \Lambda \to 0 \quad R^*(5) = 0.064\text{cm}^3.
\end{aligned}$$

Over 10 seconds:

$$\begin{aligned}
K &= 0.5 \quad \Lambda \to \infty \quad R^*(10) = 3.07\text{cm}^3 \\
K &= 0.5 \quad \Lambda \to 0 \quad R^*(10) = 3.10\text{cm}^3 \\
K &= 3.0 \quad \Lambda \to \infty \quad R^*(10) = 0.170\text{cm}^3 \\
K &= 3.0 \quad \Lambda \to 0 \quad R^*(10) = 0.201\text{cm}^3 \\
K &= 10.0 \quad \Lambda \to \infty \quad R^*(10) = 0.077\text{cm}^3 \\
K &= 10.0 \quad \Lambda \to 0 \quad R^*(10) = 0.109\text{cm}^3.
\end{aligned}$$

Over 20 seconds:

$$\begin{aligned}
K &= 0.5 \quad \Lambda \to \infty \quad R^*(20) = 5.08\text{cm}^3 \\
K &= 0.5 \quad \Lambda \to 0 \quad R^*(20) = 5.12\text{cm}^3 \\
K &= 3.0 \quad \Lambda \to \infty \quad R^*(20) = 0.291\text{cm}^3 \\
K &= 3.0 \quad \Lambda \to 0 \quad R^*(20) = 0.342\text{cm}^3 \\
K &= 10.0 \quad \Lambda \to \infty \quad R^*(20) = 0.124\text{cm}^3 \\
K &= 10.0 \quad \Lambda \to 0 \quad R^*(20) = 0.174\text{cm}^3.
\end{aligned}$$

Over 40 seconds:

$$\begin{aligned}
K &= 0.5 \quad \Lambda \to \infty \quad R^*(40) = 7.99\text{cm}^3 \\
K &= 0.5 \quad \Lambda \to 0 \quad R^*(40) = 8.05\text{cm}^3 \\
K &= 3.0 \quad \Lambda \to \infty \quad R^*(40) = 0.469\text{cm}^3 \\
K &= 3.0 \quad \Lambda \to 0 \quad R^*(40) = 0.551\text{cm}^3 \\
K &= 10.0 \quad \Lambda \to \infty \quad R^*(40) = 0.190\text{cm}^3 \\
K &= 10.0 \quad \Lambda \to 0 \quad R^*(40) = 0.268\text{cm}^3.
\end{aligned}$$

Since the volume of the adult renal pelvis is of the order of 10 cm³, the reflux values obtained for the value $K = 0.5$ are clearly unphysiological. The values corresponding to $K = 3$ and $K = 10$ are reasonable though, and (if these K-values are physiological for a stented human ureter) demonstrate that over the voiding

duration up to a 30 per cent reduction in reflux is obtained with the very porous stent.

Reflux for separable solution (6.38) Here we have

$$\frac{\partial B_1}{\partial z} = \frac{1}{K} + \sum_{n=1}^{\infty} \frac{2(-1)^n}{K} \exp(-Dn^2\pi^2 t) \cos n\pi z. \tag{7.50}$$

The expressions (7.42) and (7.43) then give the total reflux in the limit $\Lambda \to \infty$ as

$$\left(\frac{-Q}{\delta}\right)_{\Lambda \to \infty} = \frac{2\pi(K+1)D_\infty}{K^2} \left\{1 + 2\sum_{n=1}^{\infty} (-1)^n \exp(-D_\infty n^2\pi^2 t)\right\}, \tag{7.51}$$

and in the limit $\Lambda \to 0$ as

$$\left(\frac{-Q}{\delta}\right)_{\Lambda \to 0} = \frac{\pi}{8} + \frac{2\pi(K+1)D_0}{K^2} \left\{1 + 2\sum_{n=1}^{\infty} (-1)^n \exp(-D_0 n^2\pi^2 t)\right\}. \tag{7.52}$$

These expressions are plotted in figures 11, 12 and 13 which show that for small times the reflux is greater in the limit $\Lambda \to 0$, but for later times it is greater for the $\Lambda \to \infty$ stent; so it is not immediately clear which limit gives greater total reflux. By integrating in time we can evaluate the total amount of fluid that has refluxed in the time interval $(0, T)$:

$$\int_0^T \left(\frac{-Q}{\delta}\right)_{\Lambda \to \infty} dt = \frac{2\pi(K+1)}{K^2} \left\{D_\infty T + 2\sum_{n=1}^{\infty} \frac{(-1)^n}{n^2\pi^2}\right.$$
$$\left. \times (1 - \exp(-D_\infty n^2\pi^2 T))\right\}, \tag{7.53}$$

$$\int_0^T \left(\frac{-Q}{\delta}\right)_{\Lambda \to 0} dt = \frac{2\pi(K+1)}{K^2} \left\{D_\infty T + 2\sum_{n=1}^{\infty} \frac{(-1)^n}{n^2\pi^2}\right.$$
$$\left. \times (1 - \exp(-D_0 n^2\pi^2 T))\right\}. \tag{7.54}$$

As can be seen, the $O(T)$-contributions to reflux are exactly the same in both cases (the first terms within the curly brackets), and the remaining terms decay (rapidly) as T increases, so that the two expressions (7.53) and (7.54) become equal as $T \to \infty$. Considering the function

$$f(DT) := \sum_{n=1}^{\infty} \frac{(-1)^n}{n^2\pi^2} (1 - \exp(-DT n^2\pi^2)),$$

it may be seen that this is a negative, monotone decreasing, function of DT. Hence, since $D_\infty > D_0$, it follows that there is greater reflux for the $\Lambda \to 0$ stent, over any given time interval $(0, T)$. However, the difference is very small for any $O(1)$ times, as illustrated below.

Dimensional total reflux The dimensional total reflux over a time T^* is again given by (7.49). Again assuming voiding times of $T^* = 5, 10, 20, 40$s (so the dimensionless voiding times are $T \approx 2.5, 5, 10, 20$) and performing the integral numerically for various K-values, we obtain the following values for the separable solution:

Over 5 seconds:

$$K = 0.5 \quad \Lambda \to \infty, \ 0 \ R^*(5) = 3.92\text{cm}^3$$
$$K = 3.0 \quad \Lambda \to \infty, \ 0 \ R^*(5) = 0.193\text{cm}^3$$
$$K = 10.0 \ \Lambda \to \infty, \ 0 \ R^*(5) = 0.114\text{cm}^3.$$

Over 10 seconds:

$$K = 0.5 \quad \Lambda \to \infty, \ 0 \ R^*(10) = 8.23\text{cm}^3$$
$$K = 3.0 \quad \Lambda \to \infty, \ 0 \ R^*(10) = 0.415\text{cm}^3$$
$$K = 10.0 \ \Lambda \to \infty, \ 0 \ R^*(10) = 0.235\text{cm}^3.$$

Over 20 seconds:

$$K = 0.5 \quad \Lambda \to \infty, \ 0 \ R^*(20) = 16.85\text{cm}^3$$
$$K = 3.0 \quad \Lambda \to \infty, \ 0 \ R^*(20) = 0.858\text{cm}^3$$
$$K = 10.0 \ \Lambda \to \infty, \ 0 \ R^*(20) = 0.478\text{cm}^3.$$

Over 40 seconds:

$$K = 0.5 \quad \Lambda \to \infty, \ 0 \ R^*(40) = 34.10\text{cm}^3$$
$$K = 3.0 \quad \Lambda \to \infty, \ 0 \ R^*(40) = 1.746\text{cm}^3$$
$$K = 10.0 \ \Lambda \to \infty, \ 0 \ R^*(40) = 0.963\text{cm}^3.$$

In this case, the total volumes refluxed are virtually identical for all times considered, as may be deduced by considering (7.53) and (7.54). As with the similarity solution, the value $K = 0.5$ leads to reflux volumes that are clearly unphysical, while the larger K-values give reasonable reflux volumes.

8. Discussion and conclusions

We have developed a new mathematical model for urine flow in a stented kidney-ureter-bladder system. The ureter is modelled as an elastic walled tube, and the stent as a rigid permeable tube, of the same length, inside it (the end curls of the stent were ignored). Axisymmetry is assumed, which is thought not to be too unrealistic in view of the ballooning of the ureter lumen that occurs in a stented system. The flow is governed by the Navier-Stokes equations (which simplify due to the small aspect ratio of the system – lubrication theory), subject to appropriate boundary conditions at the ureter and stent walls. Since the presence of a stent abolishes peristalsis, the flow is driven solely by pressure differences between the renal pelvis and the bladder. The model results in a fourth-order system of partial differential equations relating the pressures within the stent and ureter, and the ureter radius $B(z, t)$. The key dimensionless parameters are the ureter wall stiffness, K, and the ureter wall permeability, Λ.

We considered in detail two limiting cases: large ($\Lambda \to \infty$) and small ($\Lambda \to 0$) wall permeability, to investigate what effect the holes in the stent wall have on the flow. In both cases, asymptotic expansions were exploited to find steady solutions to the governing equations which have equal reduced pressures at either end of the ureter (so the reduced pressure is constant throughout the system). This solution is appropriate to voiding (which certainly lasts long enough for a steady state to be set up), since the reduced pressures in the bladder and renal pelvis are then nearly equal. We then considered small time-dependent perturbations to this steady state, in order to capture more accurately the flow dynamics during voiding. In particular we found that, in each case, the correction to the steady-state ureter radius satisfies a simple diffusion equation, the diffusion coefficient for $\Lambda \to \infty$ being greater than that for $\Lambda \to 0$, so that perturbations take longer to decay in the limit $\Lambda \to \infty$. Simple explicit solutions to the diffusion equations were found, and thus the ureter wall shape identified.

The main focus of our study is on reflux, where bladder urine flows back up the ureter towards the renal pelvis. For those 80–85% of patients only requiring a stent in the short term, reflux is a far more serious issue than encrustation. For long-term stent patients reflux is closely linked with the encrustation problem; bladder urine has higher levels of both salts and bacteria and, since bacteria can increase urinary pH, which enhances crystal formation, reflux can accelerate encrustation in the renal pelvis.

We evaluated the reflux predicted by the model for two simple test solutions: a similarity solution, and a solution expressible as a sum of separable modes. While for both solutions the bladder pressure was assumed constant throughout (uniform squeezing of the bladder by the patient), conditions at the renal pelvis differed. The similarity solution has the feature that the pressure within the renal pelvis slowly rises as the reflux occurs, mimicking, though in an ad hoc manner, the pressure rise that would occur as the volume of fluid within the renal pelvis increases. In the separable solution, the renal pelvis pressure was held fixed, the assumption being that for only small amounts of reflux, it will not change much.

The results of the model indicate that when the bladder pressure rises sufficiently to cause reflux, the high-permeability stent gives, in all cases, *less total reflux* than the small permeability stent. This result is quite marked for the similarity solutions, the reduction in reflux being up to 30 percent for the cases we considered; but is negligible for the separable solutions. Overall our results suggest that holes are probably a good design feature as far as reflux is concerned; however, a wider range of (more realistic) solutions must be studied before we can state conclusively that holes reduce reflux.

As well as examining the effect of Λ on reflux, we are interested in how other issues depend on the wall permeability. For example, there are sometimes problems with stents fracturing *in vivo*, and it has been conjectured [4,7] that the stent holes may be partly responsible for this. Thus it is important to quantify the differences in the flow as Λ varies, in order to draw conclusions as to the usefulness of the holes.

We assumed throughout that the stent is uniformly permeable, but there is no reason why we cannot allow Λ also to vary with z. In particular, this will be the

case after a stent has been in position for some time, as holes will become blocked by encrustation (see Introduction). Allowing Λ to vary with z will also allow us to investigate different 'hole patterns', to see whether there is an optimal design as regards minimising reflux. In future we intend to carry out a comprehensive study of flow behaviour for arbitrary permeability (rather than the two extreme cases considered here), and for a variable Λ to mimic the encrustation.

Finally, as derived in §2.4, the ureter stiffness K is assumed to be a function of distance z along the ureter, allowing us to model an external blockage in the ureter as a section along which K is large. However, our analysis has concentrated on the case of constant ureter stiffness K, thus strictly speaking, our results are really valid only for healthy stented ureters, or uniformly blocked ureters. This is clearly a shortcoming of our analysis, and in a forthcoming publication we investigate the effect of variable ureter stiffness.

References

1. Carew, E.O., Pedley, T.J.: An active membrane model for peristaltic pumping: Part I – Periodic activation waves in an infinite tube. J. Biomech. Eng. **119**, 66–76 (1997)
2. Culkin, D.J., Zitman, R., Bundrick, W.S., Goel, Y., Price, V.H., Ledbetter, S., Mata, J.A., Venable, D.D.: Anatomical, functional, and pathologic changes from internal ureteral stent placement. Urol. **40** (4), 385–390 (1992)
3. Dauleh, M.J., Byrne, D.J., Baxby, K.: Non-refluxing minimal irritation ureteric stent. Br. J. Urol. **76**, 795–796 (1995)
4. Elsherif, A.: Fracture of polyurethane double pigtail stents – an in vivo retrospective and prospective fluoroscopic study. Br. J. Urol. **76** (1), 108–114 (1995)
5. Finney, R.P.: Experience with new double-J ureteral catheter stent. J. Urol. **120**, 678–681 (1978)
6. Gorman, S.P., Tunney, M.M.: Assessment of encrustation behaviour on urinary tract biomaterials. J. Biomat. App. **12**, 136–166 (1997)
7. Gorman, S.P., Jones, D.S., Bonner, M.C., Akay, M., Keane, P.F.: Mechanical performance of polyurethane ureteral stents in vitro and ex vivo. Biomat. **18** (20), 1379–1383 (1997)
8. Griffiths, D.J.: Dynamics of the upper urinary tract: I. Peristaltic flow through a distensible tube of limited length. Phys. Med. Biol. **32** (7), 813–822 (1987)
9. Griffiths, D.J., Constantinou, C.E., Mortensen, J., Djurhuus, J.C.: Dynamics of the upper urinary tract: II. The effect of variations of peristaltic frequency and bladder pressure on pyeloureteral pressure/flow relations. Phys. Med. Biol. **32** (7), 823–833 (1987)
10. Knudsen, L., Gregerson, H., Eika, B., Frøkiær, J.: Elastic wall properties and collagen content in the ureter: An experimental study in pigs. Neurourol. Urodyn. **13**, 597–608 (1994)
11. Mundy, A.R., Stephenson, T.P., Wein, A.J.: (Editors). Urodynamics: principles, practice and application. 2nd ed. Edinburgh: Churchill Livingstone, 1994

12. Nancollis, G.H.: Crystallisation theory relating to urinary stone formation. World J. Urol. **1**, 131–137 (1983)
13. Patel, U., Kellett, M.J.: Ureteric drainage and peristalsis after stenting studied using colour Doppler ultrasound. Br. J. Urol. **77**, 530–535 (1996)
14. Seymour, H., Patel, U.: Ureteric stenting - Current status. Semin. Intervent. Radiol. **17**, 351–366 (2000)